Supporting Information

Promotional Effect of Indium on the CuO-CeO$_2$ Catalysts for Low-Temperature CO Oxidation

Hu Li[a], Fei-Xiang Tian[a], Qi Liu[a], Yi-Fan Han[a,*] and Minghui Zhu[a,*]

[a] State Key Laboratory of Chemical Engineering, School of Chemical Engineering, East China University of Science and Technology, Shanghai 200237, China

[*] Corresponding author E-mail: yifanhan@ecust.edu.cn; minghuizhu@ecust.edu.cn

. **Supplementary figures**

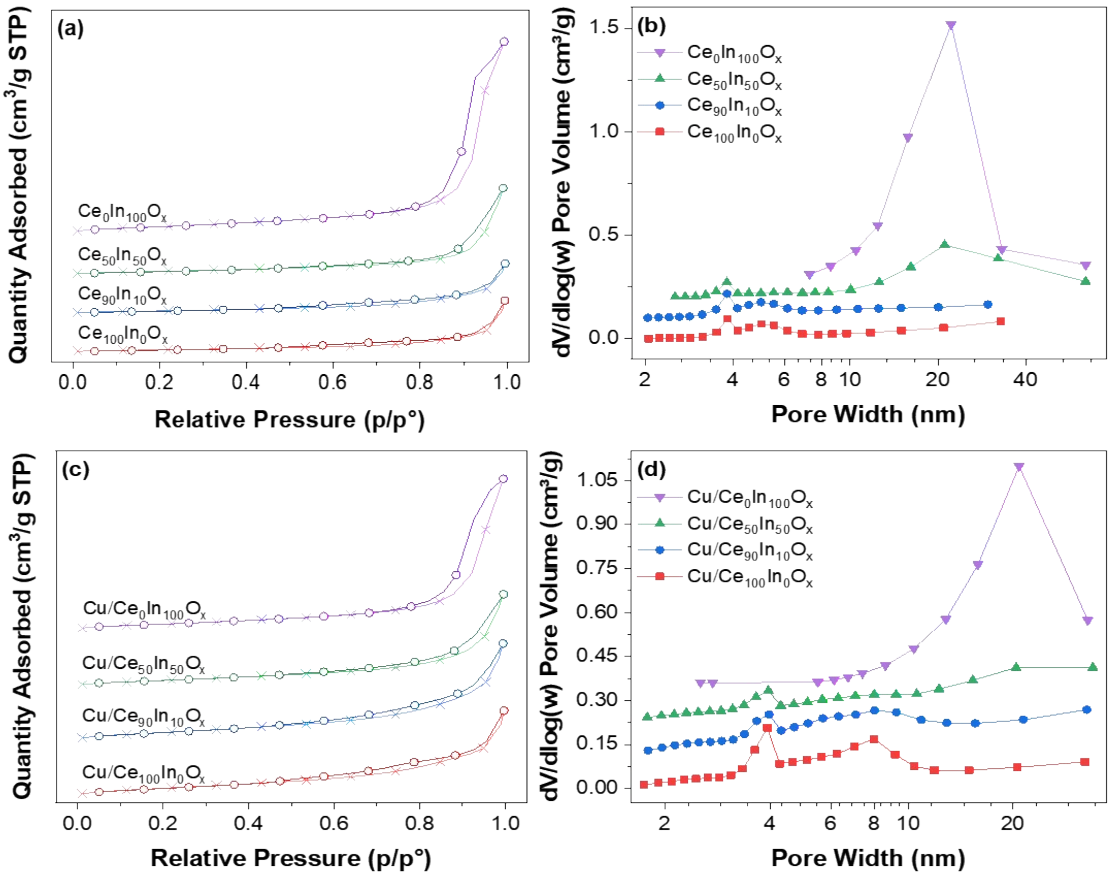

Figure S1. N_2 adsorption/desorption isotherms and pore size distributions of $CeInO_x$ (a-b) supports and Cu/$CeInO_x$ (c-d) catalysts.

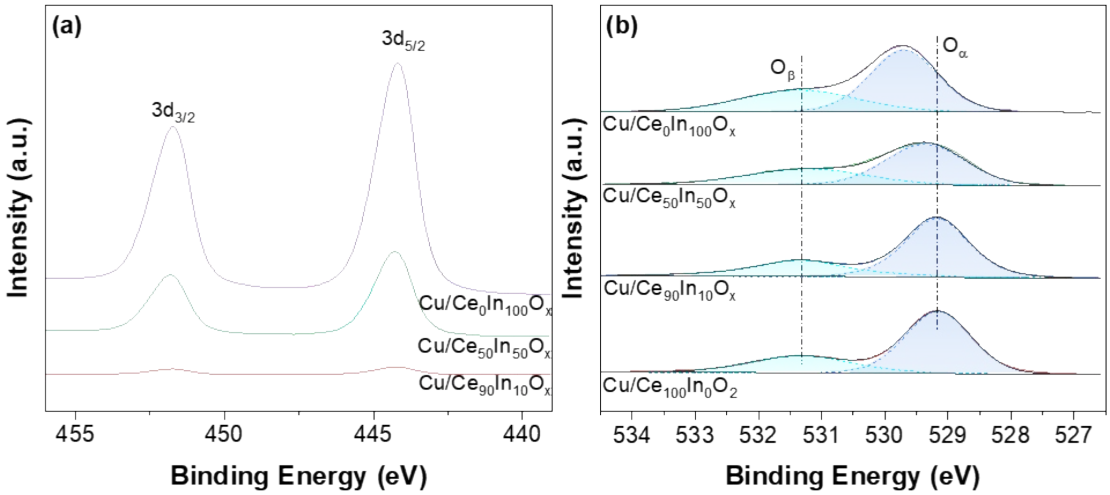

Figure S2. XPS spectra of the catalysts showing the (a) O 1s, (b) In 3d regions.

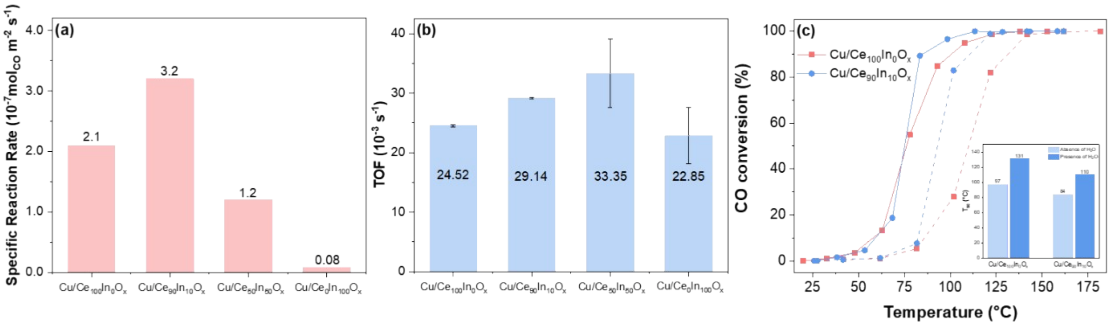

Figure S3. (a) Specific reaction rate and (b) TOF in the absence of 3 vol.% H_2O over Cu/CeInO_x catalysts at 90 °C. (c) Effect of H_2O on CO conversion over Cu/CeInO_x catalysts.

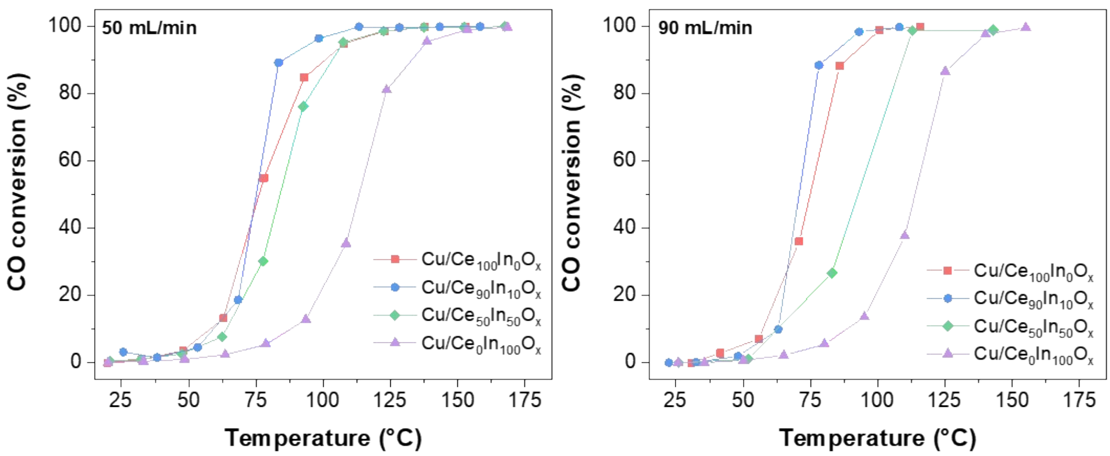

Figure S4. CO conversion of Cu/CeInO_x catalysts at different flow rates (50 and 90 mL·min^{-1}).

CO-TPD was also performed using the same micro-fixed-bed reactor connected to a GC-QMS (HPR-20, Hiden Analytical Ltd.). The pretreatment procedure was identical to the H_2-TPR experiment. First, 50 mg catalyst was cooled down to room temperature in flowing Ar (Air Liquid, 99.999%). The catalyst was then saturated under a CO flow (1%CO/Ar) for 1 h and purged with Ar for 1.5 h to remove physically adsorbed CO molecules. The temperature was then ramped up to 850 °C at a rate of 10 °C·min^{-1}.

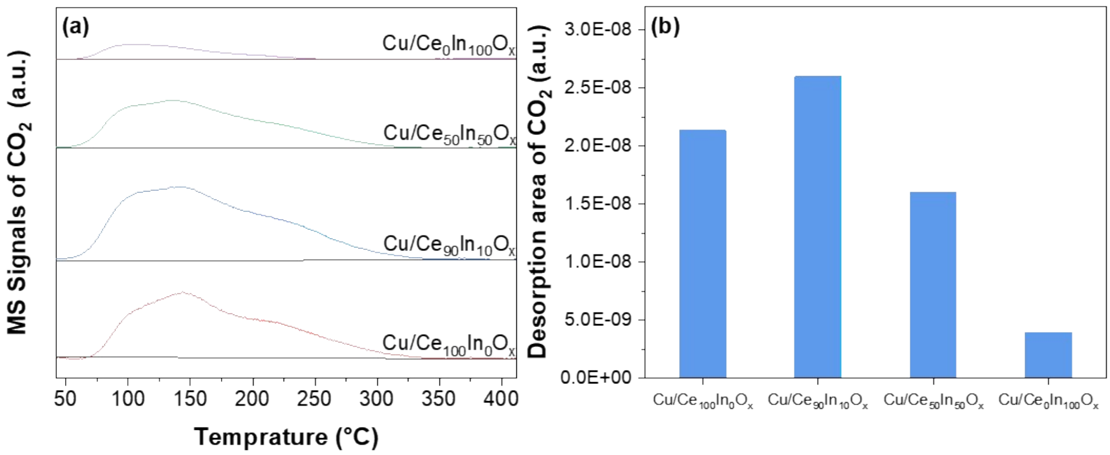

Figure S5. (a) CO-TPD profiles of Cu/CeInO$_x$ catalysts. (b) Desorption area of CO_2 during CO-TPD over Cu/CeInO$_x$ catalysts.

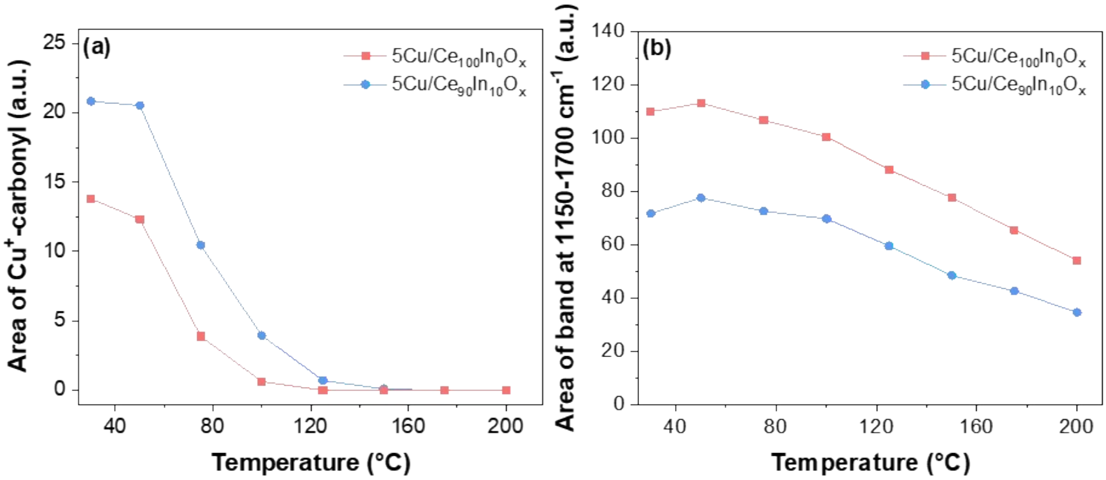

Figure S6. Integrated area of (a) CO-Cu^+ species and (b) the carbon-containing species in the 1150-1700 cm^{-1} range as a function of the reaction temperature.

Scanning transmission electron microscopy (STEM) measurement was carried out on a ThermoFisher Talos F200X (Figure S7). Energy-dispersive X-ray spectroscopy (EDX) measurement was performed using 4 in-column Super-X detectors (Figure S8).

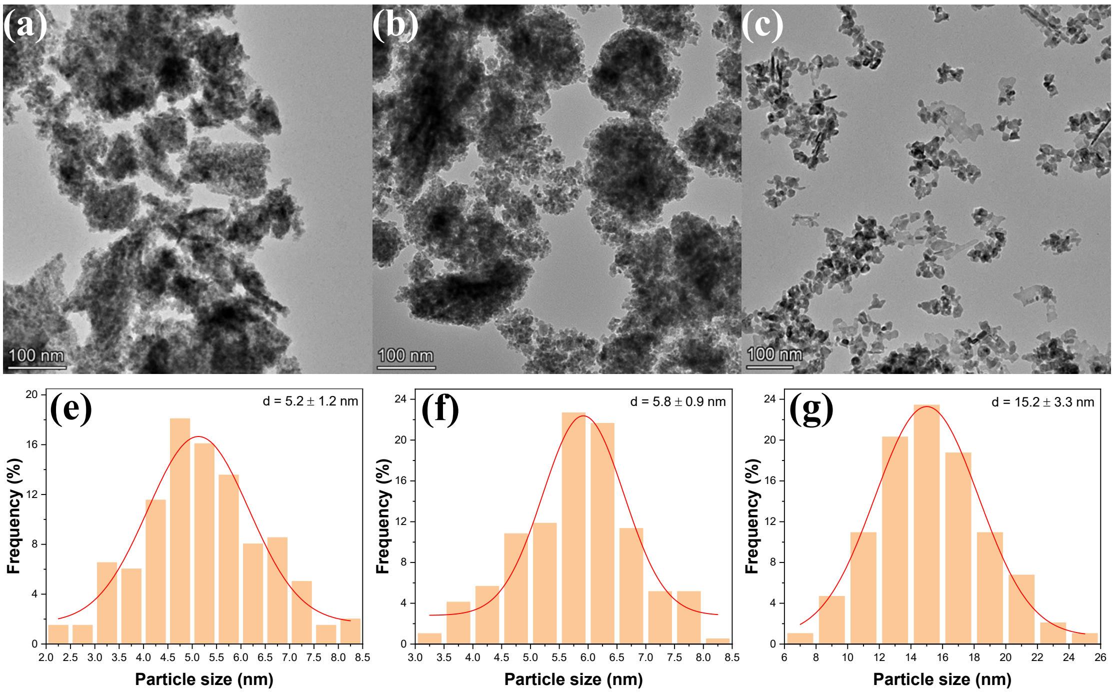

Figure S7. TEM images and the size distribution of different catalysts: (a, e) $Cu/Ce_{100}In_0O_x$, (b, f) $Cu/Ce_{90}In_{10}O_x$, and (c, g) $Cu/Ce_0In_{100}O_x$.

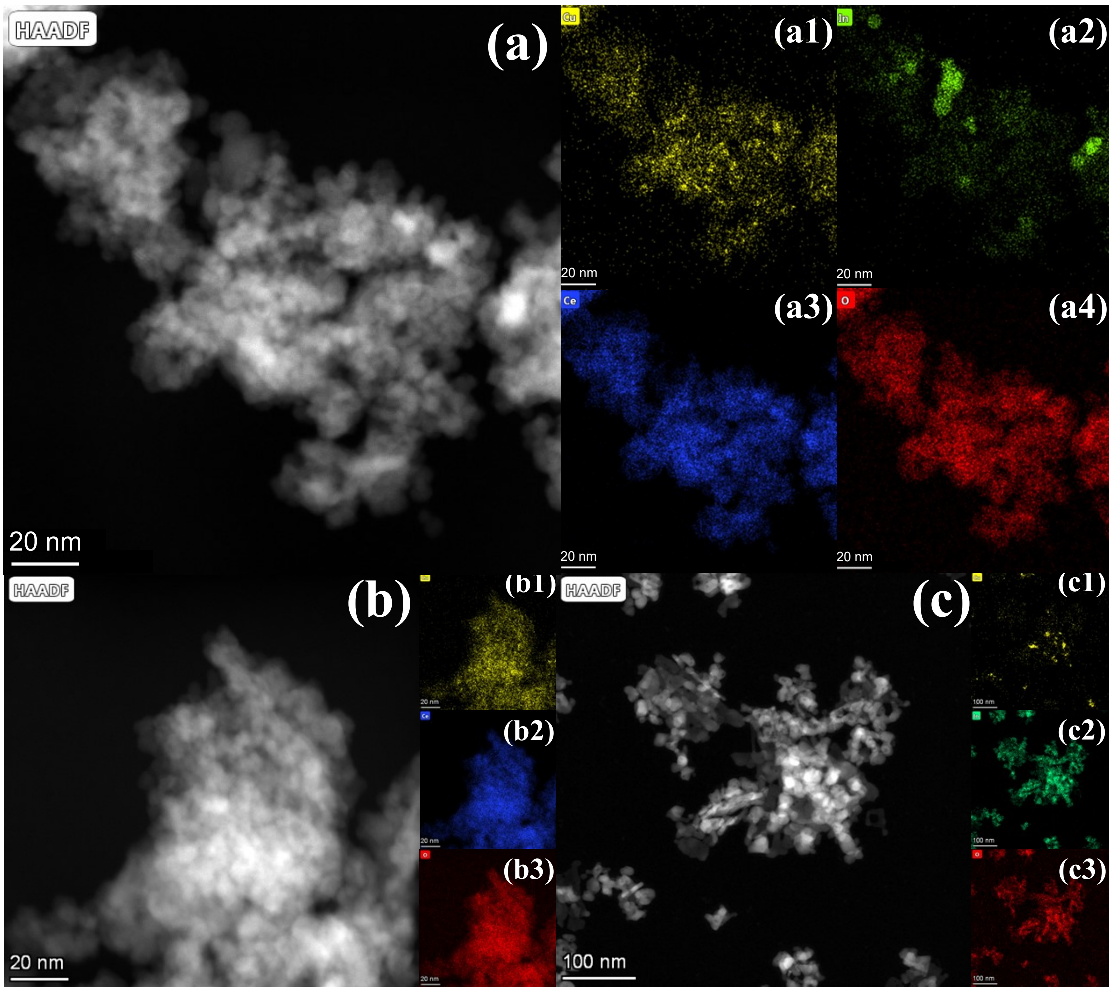

Figure S8. EDX-Mapping results of (a) $Cu/Ce_{90}In_{10}O_x$, (b) $Cu/Ce_{100}In_0O_x$, and (c) $Cu/Ce_0In_{100}O_x$. The yellow, green, blue and red represent Cu, In, Ce and O, respectively.

Supplementary tables

Table S1

The BET surface area, Barrett Joiner Halenda (BJH) pore volume, and pore size for the supports and catalysts.

Sample	Surface area (m^2/g)	Pore volume (cm^3/g)	Pore size (nm)
$Ce_{100}In_0O_x$	20.9	0.067	10.6
$Ce_{90}In_{10}O_x$	24.3	0.068	9.1
$Ce_{50}In_{50}O_x$	30.3	0.181	20.4
$Ce_0In_{100}O_x$	60.0	0.401	20.4
$Cu/Ce_{100}In_0O_x$	66.7	0.118	6.9
$Cu/Ce_{90}In_{10}O_x$	66.3	0.159	8.8
$Cu/Ce_{50}In_{50}O_x$	48.5	0.148	11.4
$Cu/Ce_0In_{100}O_x$	49.5	0.281	19.2

Table S2

The unit cell parameters and particle size of the supports and catalysts as determined by TOPAS. Results of the Sample Characterization by XRD.

Sample	CeO_2 lattice parameters (nm)	particle size (nm)	
		CeO_2	In_2O_3
$Ce_{100}In_0O_x$	0.5419	7.7	-
$Ce_{90}In_{10}O_x$	0.5416	8.2	-
$Ce_{50}In_{50}O_x$	0.5401	7.1	15.2
$Ce_0In_{100}O_x$	-	-	16.8
$Cu/Ce_{100}In_0O_x$	0.5418	7.9	-
$Cu/Ce_{90}In_{10}O_x$	0.5419	7.2	-
$Cu/Ce_{50}In_{50}O_x$	0.5399	7.3	15.3
$Cu/Ce_0In_{100}O_x$	-	-	17.0

Table S3

Quantified XPS Results for the catalysts.

Catalyst	Cu (mol %)	Ce^{3+}/Ce (%)	I_{sat}/I_{pp}	Cu^{+}/Cu (%)
$Cu/Ce_{100}In_0O_x$	9.07	20.9	0.128	60.4
$Cu/Ce_{90}In_{10}O_x$	10.29	21.3	0.098	66.7
$Cu/Ce_{50}In_{50}O_x$	7.27	13.6	0.125	59.0
$Cu/Ce_0In_{100}O_x$	4.43	-	0.114	55.6

Table S4

The residual Na content of the $Cu/Ce_{90}In_{10}O_x$ and $Cu/Ce_{50}In_{50}O_x$ catalyst by ICP-OES.

Catalyst	0722-Na (wt.%)	0915-Na (wt.%)
$Cu/Ce_{90}In_{10}O_x$	0.421	0.295
$Cu/Ce_{50}In_{50}O_x$	0.381	0.095

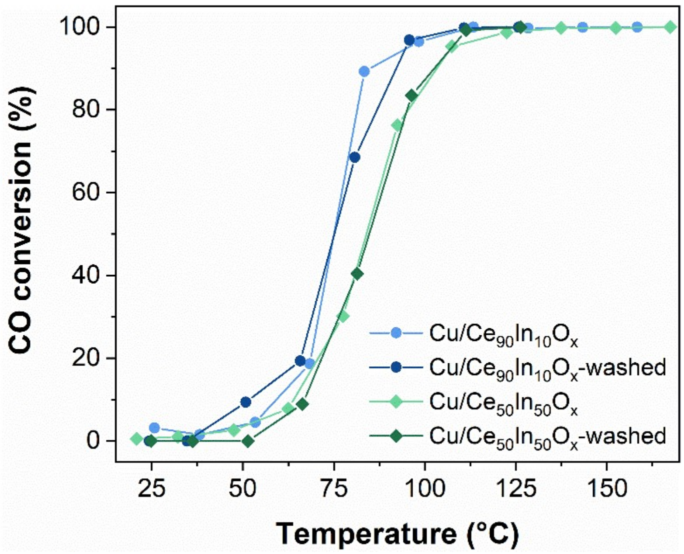

Figure S9. CO conversion of the $Cu/Ce_{90}In_{10}O_x$ and $Cu/Ce_{50}In_{50}O_x$ catalysts with different residual Na.

We have determined the residual Na content of the $Cu/Ce_{90}In_{10}O_x$ and $Cu/Ce_{50}In_{50}O_x$ catalysts prepared on July 22 and September 15 by ICP-OES (PE Avio200) (Table S4). ICP results show that the extensive washing step somewhat successfully removes Na. Steady-state activity measurements reveal that removal (or partial removal) of Na from these catalysts shows almost negligible impact on the CO oxidation activity especially under lower temperatures (Figure S9).